

Heat transport by turbulent Rayleigh-Bénard Convection in cylindrical samples with aspect ratio one and larger

By Denis Funfschilling, Eric Brown, Alexei Nikolaenko, and Guenter Ahlers

Department of Physics and iQUEST,
University of California, Santa Barbara, CA 93106

(Received 8 August 2018)

We present high-precision measurements of the Nusselt number \mathcal{N} as a function of the Rayleigh number R for cylindrical samples of water (Prandtl number $\sigma = 4.38$) with diameters $D = 49.7, 24.8$, and 9.2 cm, all with aspect ratio $\Gamma \equiv D/L \simeq 1$ (L is the sample height). In addition, we present data for $D = 49.7$ and $\Gamma = 1.5, 2, 3$, and 6 . For each sample the data cover a range of a little over a decade of R . For $\Gamma \simeq 1$ they jointly span the range $10^7 \lesssim R \lesssim 10^{11}$. Where needed, the data were corrected for the influence of the finite conductivity of the top and bottom plates and of the side walls on the heat transport in the fluid to obtain estimates of \mathcal{N}_∞ for plates with infinite conductivity and sidewalls of zero conductivity. For $\Gamma \simeq 1$ the effective exponent γ_{eff} of $\mathcal{N}_\infty = N_0 R^{\gamma_{eff}}$ ranges from 0.28 near $R = 10^8$ to 0.333 near $R \simeq 7 \times 10^{10}$. For $R \lesssim 10^{10}$ the results are consistent with the Grossmann-Lohse model. For larger R , where the data indicate that $\mathcal{N}_\infty(R) \sim R^{1/3}$, the theory has a smaller γ_{eff} than $1/3$ and falls below the data. The data for $\Gamma > 1$ are only a few percent smaller than the $\Gamma = 1$ results.

1. Introduction

A central prediction of theoretical models of turbulent Rayleigh-Bénard convection (RBC) in a fluid heated from below [Kraichnan(1962), Siggia(1994), Kadanoff(2001), Ahlers, Grossmann & Lohse (2002), Grossmann & Lohse (2000)] is the dependence of the global heat transport on the Rayleigh number

$$R = \alpha g \Delta T L^3 / \kappa \nu \quad (1.1)$$

(α is the isobaric thermal expansion coefficient, κ the thermal diffusivity, ν the kinematic viscosity, g the acceleration of gravity, ΔT the temperature difference, and L the sample height) and the Prandtl number $\sigma = \nu/\kappa$. The heat transport is usually expressed in terms of the Nusselt number

$$\mathcal{N} = QL/\lambda\Delta T \quad (1.2)$$

where Q is the heat-current density and λ is the thermal conductivity of the fluid in the absence of convection. Before a quantitative comparison between theory and experiment can be made, the results for \mathcal{N} usually must be corrected for the influence of the side wall [Ahlers(2000), Roche *et al.*(2001), Niemela & Sreenivasan (2003)] and the top and bottom plates [Chaumat *et al.*(2002), Verzicco(2004), Brown *et al.* (2005)] to yield an estimate of the idealized \mathcal{N}_∞ .

A model developed recently by Grossmann & Lohse (2000), based on the decomposition

No	$\bar{T}(^{\circ}C)$	$\Delta T(^{\circ}C)$	$10^{-8}R$	\mathcal{N}	\mathcal{N}_{∞}	No	$\bar{T}(^{\circ}C)$	$\Delta T(^{\circ}C)$	$10^{-8}R$	\mathcal{N}	\mathcal{N}_{∞}
1	40.009	1.957	94.3	127.0	129.3	2	40.011	3.911	188.6	157.5	161.4
3	39.984	5.917	285.0	179.4	184.8	4	40.007	7.821	377.0	195.8	202.5
5	40.007	9.764	470.7	210.1	218.0	6	40.022	11.676	563.1	222.3	231.3
7	40.039	13.589	655.7	233.5	243.6	8	39.955	15.688	754.8	243.7	254.9
9	39.901	17.729	851.4	253.4	265.6	10	39.887	19.705	945.8	261.8	274.9
11	40.041	6.783	327.3	187.5	193.5	12	40.062	4.791	231.4	167.9	172.5
13	40.056	2.849	137.6	142.8	145.9	14	39.963	2.543	122.4	137.5	140.3
15	39.944	1.595	76.7	118.5	120.4	16	39.923	19.623	943.0	261.7	274.7
17	39.921	19.627	943.2	261.6	274.7	18	39.929	5.048	242.7	170.6	175.4
19	39.970	1.050	50.6	104.6	106.0	20	39.999	9.775	471.1	210.3	218.2
21	39.998	9.782	471.4	210.3	218.3	22	40.016	0.962	46.4	101.8	103.1
23	40.015	0.963	46.4	101.9	103.2	24	39.904	19.666	944.5	261.7	274.8
25	39.963	2.539	122.2	137.6	140.4	26	40.000	1.485	71.5	116.3	118.1
27	40.011	1.954	94.2	127.0	129.2	28	40.011	1.955	94.3	126.9	129.2
29	40.010	1.954	94.2	126.9	129.1	30	39.993	1.005	48.4	103.1	104.4
31	39.859	21.687	1040.0	269.4	283.3	32	39.971	3.988	192.0	158.4	162.4

TABLE 1. Results for $\Gamma = 0.982$, run 2 from the large apparatus ($D = 49.7$ cm). In Table 1 to 7 two points are listed per line, and they are numbered in chronological sequence.

of the kinetic and the thermal dissipation into boundary-layer and bulk contributions, provided a good fit to experimental data [Xu, Bajaj & Ahlers(2000), Ahlers & Xu (2001)] for a cylindrical sample of aspect ratio $\Gamma \equiv D/L = 1$ (D is the diameter) when it was adapted [Grossmann & Lohse (2001), GL] to the relatively small Reynolds numbers of the measurements. However, the data were used to determine four adjustable parameters of the model. Thus more stringent tests using measurements for the same Γ but over wider ranges of R and σ are desirable. A success of the model was the agreement with recent results by Xia, Lam & Zhou(2002) for much larger Prandtl numbers than those of Ahlers & Xu (2001), for $R = 1.78 \times 10^7$ and 1.78×10^9 . It is the primary aim of the present paper to extend the range of R over which high-precision data, subject to minimal systematic errors, are available for $\mathcal{N}_{\infty}(R)$. Our data span the range $10^7 \lesssim R \lesssim 10^{11}$ with $\sigma = 4.38$ and $\Gamma \simeq 1$ and deviate from the Boussinesq approximation (Boussinesq (1903)) by less than a few tenths of a percent. We believe that they can serve as a benchmark for comparison with future experimental and theoretical developments. They agree quite well with the GL model for $R \lesssim 10^{10}$, but for larger R there are deviations.

In addition to the results for $\Gamma \simeq 1$ we present also some data for larger Γ , up to $\Gamma = 6$. We find that there is remarkably little dependence of \mathcal{N} on Γ . For instance, the $\Gamma = 6$ data fall only about 4% below the $\Gamma = 1$ results.

2. Problems associated with high-precision measurements of \mathcal{N}

One problem in the measurements of $\mathcal{N}(R)$ is that data with a precision of 0.1% or so can be obtained in a given sample only over a range of R covering a little more than a decade unless the fluid is changed. The reason is that the useful temperature differences with conventional fluids like water are limited at the high end to $\Delta T \lesssim 15^{\circ}C$ by possible contributions from non-Boussinesq effects (Boussinesq (1903)) and at the low end to $\Delta T \gtrsim 1^{\circ}C$ by thermometer resolution. For this reason we built three apparatus containing samples of diameter $D = 49.7, 24.8,$ and 9.2 cm, all with $\Gamma \simeq 1$ and known as the large, medium, and small apparatus or sample respectively (Brown et al. (2005)). Together the data obtained with these span the range $10^7 \lesssim R \lesssim 10^{11}$.

No	$\bar{T}(^{\circ}C)$	$\Delta T(^{\circ}C)$	$10^{-8}R$	\mathcal{N}	\mathcal{N}_{∞}	No	$\bar{T}(^{\circ}C)$	$\Delta T(^{\circ}C)$	$10^{-8}R$	\mathcal{N}	\mathcal{N}_{∞}
1	39.985	2.002	11.3	66.5	66.6	2	40.014	2.437	13.7	70.5	70.6
3	40.003	3.147	17.7	76.0	76.2	4	39.968	4.005	22.6	81.7	81.9
5	39.987	4.951	27.9	87.2	87.5	6	39.973	6.202	34.9	93.3	93.7
7	39.994	7.679	43.3	99.6	100.1	8	39.946	9.731	54.8	107.0	107.6
9	39.956	11.862	66.8	113.7	114.5	10	39.928	14.259	80.2	120.3	121.2
11	39.911	16.824	94.6	126.5	127.6	12	39.865	19.836	111.3	133.1	134.5
13	39.979	1.618	9.1	62.4	62.5	14	39.998	1.282	7.2	58.3	58.3
15	39.970	1.041	5.9	54.8	54.9	16	39.968	0.845	4.8	51.6	51.6
17	39.967	0.650	3.7	47.7	47.7	18	39.989	0.507	2.9	44.4	44.5
19	39.954	22.581	127.1	138.7	140.2	20	39.959	23.539	132.6	140.4	142.0
21	39.948	25.499	143.5	143.9	145.6	22	39.942	28.420	159.9	148.7	150.7
23	39.943	31.330	176.3	153.2	155.4	24	39.936	34.193	192.4	157.4	159.7
25	39.944	37.110	208.9	161.2	163.7	26	39.960	39.968	225.1	164.8	167.5

TABLE 2. Results for $\Gamma = 1.003$ from the medium apparatus ($D = 24.84$ cm).

No	$\bar{T}(^{\circ}C)$	$\Delta T(^{\circ}C)$	$10^{-6}R$	\mathcal{N}	\mathcal{N}_{∞}	No	$\bar{T}(^{\circ}C)$	$\Delta T(^{\circ}C)$	$10^{-8}R$	\mathcal{N}	\mathcal{N}_{∞}
1	39.995	0.571	18.46	20.68	20.33	2	39.995	0.721	23.34	22.13	21.76
3	39.995	0.914	29.58	23.86	23.47	4	39.995	1.160	37.53	25.51	25.11
5	39.995	1.473	47.64	27.35	26.94	6	39.995	1.871	60.52	29.28	28.86
7	39.995	2.378	76.92	31.31	30.91	8	39.995	3.025	97.85	33.57	33.13
9	39.995	3.846	124.44	35.93	35.50	10	39.996	4.894	158.35	38.44	38.00
11	39.996	6.229	201.52	41.17	40.71	12	39.996	7.927	256.49	44.02	43.55
13	39.998	10.092	326.53	47.08	46.60	14	39.999	12.848	415.73	50.35	49.87
15	39.999	16.357	529.28	53.97	53.49	16	40.002	20.823	673.87	57.80	57.30
17	40.035	26.550	860.19	61.92	61.41	18	40.054	33.658	1091.23	66.23	65.71
19	40.025	33.727	1092.34	66.37	65.85	20	40.021	35.710	1156.37	67.41	66.90
21	40.051	37.630	1219.84	68.45	67.93	22	40.080	39.579	1284.33	69.41	68.90

1	39.996	0.636	20.58	21.23	20.88	2	39.996	1.026	33.21	24.44	24.06
3	39.997	1.660	53.70	28.13	27.72	4	39.999	2.691	87.08	32.23	31.81
5	40.002	4.348	140.72	37.00	36.56	6	40.007	7.044	227.98	42.43	41.98
7	40.008	11.433	370.05	48.69	48.19	8	40.018	18.527	599.87	55.89	55.39
9	40.049	30.001	972.45	64.19	63.68	10	40.065	39.567	1283.28	69.68	69.16

TABLE 3. Results for $\Gamma = 0.967$ from the small apparatus ($D = 9.21$ cm). Top section: run 1. Bottom section: run 2 after the sample had been taken apart and re-assembled.

A second experimental problem is the influence of the side wall on the heat transport by the fluid (Ahlers(2000), Roche *et al.*(2001), Niemela & Sreenivasan (2003)). Because of the nonlinear temperature profile in the wall adjacent to the thermal boundary layers in the fluid, the heat entering (leaving) the wall at the bottom (top) can be much larger than an estimate based on a constant temperature gradient. In the present work we substantially reduced this problem by choosing a wall of small conductivity (plexiglas or lexan) and a fluid of relatively large conductivity (water). An estimate [model 2 of Ahlers(2000)] indicated that the side-wall corrections for the large and medium samples were less than a few tenths of a percent; they were neglected. For the small sample the correction was 1.7% for $R = 2 \times 10^7$ and smaller at larger R , and was made [Brown *et al.* (2005)] using model 2 of Ahlers(2000). We believe that for all the data the systematic errors due to the side-wall correction is significantly less than one percent.

A third problem is the effect of the finite conductivity λ_p of the confining top and

No	$\bar{T}(^{\circ}C)$	$\Delta T(^{\circ}C)$	$10^{-8}R$	\mathcal{N}	\mathcal{N}_{∞}	No	$\bar{T}(^{\circ}C)$	$\Delta T(^{\circ}C)$	$10^{-8}R$	\mathcal{N}	\mathcal{N}_{∞}
1	39.901	17.562	233.67	164.7	172.6	2	40.012	15.429	206.09	158.5	165.7
3	39.898	13.727	182.62	152.6	159.2	4	39.986	11.633	155.24	145.1	151.0
5	39.956	9.763	130.14	137.4	142.6	6	39.959	7.837	104.48	128.4	132.8
7	40.089	5.663	75.85	116.2	119.7	8	39.984	3.928	52.42	103.6	106.2
9	40.010	1.939	25.90	83.5	85.0	10	39.970	1.041	13.88	69.3	70.2
11	39.959	3.006	40.08	95.4	97.5	12	40.031	4.803	64.19	110.3	113.3
13	40.252	6.302	84.89	120.4	124.2	14	39.905	17.563	233.71	164.6	172.4
15	39.944	8.837	117.75	132.9	137.7						

1	39.822	19.669	260.43	170.5	179.1	2	39.827	17.730	234.80	165.3	173.3
3	40.025	13.517	180.25	152.1	158.6	4	41.676	12.258	172.99	150.4	156.8
5	40.083	7.623	101.86	127.5	131.8	6	39.973	5.900	78.53	117.6	121.2
7	40.005	3.901	51.98	103.5	106.1	8	40.008	1.948	25.96	83.6	85.1
9	40.051	2.838	37.88	93.8	95.8						

TABLE 4. Results for $\Gamma = 1.506$ from the large apparatus ($D = 49.7$ cm). Top section: run 1. Bottom section: run 2 after the sample had been taken apart and re-assembled.

No	$\bar{T}(^{\circ}C)$	$\Delta T(^{\circ}C)$	$10^{-6}R$	\mathcal{N}	\mathcal{N}_{∞}	No	$\bar{T}(^{\circ}C)$	$\Delta T(^{\circ}C)$	$10^{-8}R$	\mathcal{N}	\mathcal{N}_{∞}
1	40.012	1.944	1097.6	63.86	65.06	2	39.993	3.932	2218.8	79.11	81.17
3	40.104	5.660	3206.3	88.60	91.31	4	39.982	7.846	4426.2	97.92	101.37
5	39.981	9.789	5521.8	104.75	108.79	6	40.034	11.626	6570.7	110.63	115.22
7	39.929	13.777	7757.4	116.43	121.58	8	39.483	14.643	8116.3	117.92	123.23
9	39.977	10.767	6072.7	107.91	112.24	10	40.056	6.732	3807.7	93.38	96.47
11	40.045	4.802	2715.1	84.25	86.66	12	39.966	3.011	1697.7	72.74	74.41
13	39.972	1.041	587.2	52.83	53.55	14	39.961	17.593	9917.0	125.58	131.70

TABLE 5. Results for $\Gamma = 2.006$ from the large apparatus ($D = 49.7$ cm).

No	$\bar{T}(^{\circ}C)$	$\Delta T(^{\circ}C)$	$10^{-6}R$	\mathcal{N}	\mathcal{N}_{∞}	No	$\bar{T}(^{\circ}C)$	$\Delta T(^{\circ}C)$	$10^{-8}R$	\mathcal{N}	\mathcal{N}_{∞}
1	39.990	17.576	2937.8	85.32	89.59	2	40.007	17.578	2939.7	85.40	89.68
3	40.100	15.454	2592.9	82.13	86.04	4	39.974	13.743	2295.8	79.17	82.76
5	40.062	11.622	1947.5	75.26	78.47	6	39.978	9.839	1643.8	71.42	74.26
7	40.030	5.839	977.3	60.99	62.94	8	40.002	3.928	656.9	54.02	55.48
9	40.016	1.941	324.7	43.75	44.61	10	39.974	1.040	173.8	36.41	36.94
11	40.063	2.830	474.2	48.99	50.14	12	40.054	4.807	805.2	57.47	59.17
13	40.283	6.311	1065.7	62.65	64.74	14	39.987	8.846	1478.4	69.18	71.82

TABLE 6. Results for $\Gamma = 3.010$ from the large apparatus ($D = 49.7$ cm).

bottom plates on the heat transport by the fluid [Chaumat *et al.*(2002), Verzicco(2004), Chillà *et al.*(2004a)]. We investigated this effect experimentally [Brown *et al.* (2005)] by making measurements for samples of different sizes and aspect ratios, each with copper plates ($\lambda_p = 391$ W/m K) and with aluminum plates ($\lambda_p = 161$ W/m K). For the large and medium apparatus a small difference between the data sets enabled us to derive a correction factor. When applied to the data taken with the copper plates it yielded an increase of less than 5% for the large and less than 1% for the medium apparatus and gave a good estimate of the idealized \mathcal{N}_{∞} . For the small apparatus the results obtained with copper and aluminum plates agreed with each other.

No	$\bar{T} (^{\circ}\text{C})$	$\Delta T (^{\circ}\text{C})$	$10^{-6}R$	\mathcal{N}	\mathcal{N}_{∞}	No	$\bar{T} (^{\circ}\text{C})$	$\Delta T (^{\circ}\text{C})$	$10^{-8}R$	\mathcal{N}	\mathcal{N}_{∞}
1	40.000	19.734	412.4	46.09	48.62	2	39.977	17.804	371.8	44.74	47.11
3	39.402	16.991	347.7	43.83	46.09	4	40.134	13.567	284.9	41.32	43.31
5	40.058	11.727	245.6	39.58	41.37	6	40.054	9.781	204.8	37.51	39.10
7	40.137	7.637	160.4	34.95	36.30	8	40.015	5.920	123.8	32.38	33.51
9	40.032	3.909	81.8	28.73	29.57	10	40.019	1.944	40.7	23.62	24.14
11	40.071	2.839	59.5	26.26	26.94	12	40.085	4.791	100.4	30.49	31.47
13	40.070	6.800	142.5	33.72	34.96	14	40.051	3.375	70.7	27.55	28.31

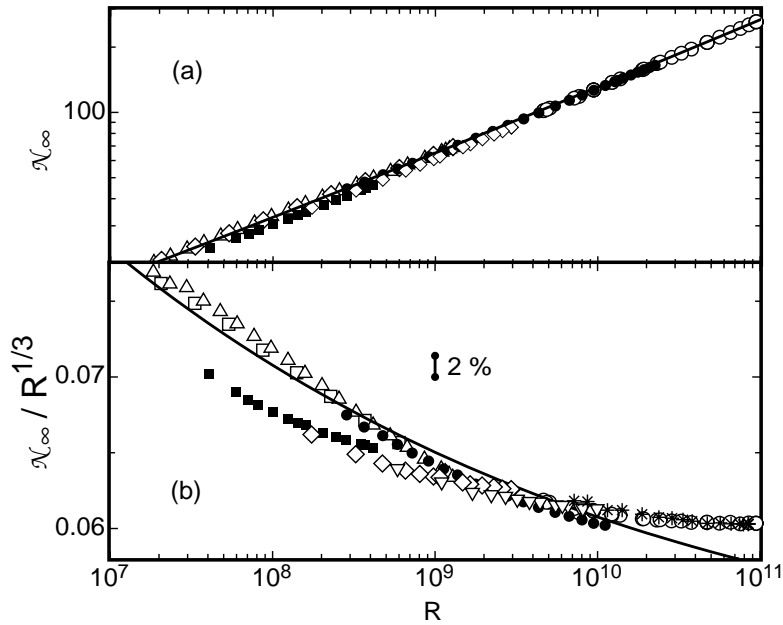
TABLE 7. Results for $\Gamma = 6.020$ from the large apparatus ($D = 49.7$ cm).

FIGURE 1. (a) The Nusselt number \mathcal{N}_{∞} as a function of the Rayleigh number R on logarithmic scales. (b) The reduced Nusselt number $\mathcal{N}_{\infty}/R^{1/3}$ on a linear scale as a function of the Rayleigh number R on a logarithmic scale. Stars: $\Gamma = 0.982$, $D = 49.7$ cm, run 1 (from Nikolaenko *et al.* (2005), corrected for a 0.5% error in the cross sectional area of the sample). Open circles: $\Gamma = 0.982$, $D = 49.7$ cm, run 2. Solid circles: $\Gamma = 1.003$, $D = 24.84$ cm. Open squares (up-pointing triangles): $\Gamma = 0.967$, $D = 9.21$ cm, run1 (run2). Open down-pointing triangles: $\Gamma = 2.006$, $D = 49.7$ cm. Open diamonds: $\Gamma = 3.010$, $D = 49.7$ cm. Solid squares: $\Gamma = 6.020$, $D = 49.7$ cm. Solid line: the model of Grossmann & Lohse (2001) for $\Gamma = 1$ and $\sigma = 4.38$.

3. Results

3.1. The data

The measurements were made at a mean temperature of 40°C , where $\sigma = 4.38$, $\kappa = 1.52 \times 10^{-7} \text{ m}^2/\text{s}$, $\nu = 6.70 \times 10^{-7} \text{ m}^2/\text{s}$, $\alpha = 3.88 \times 10^{-4} \text{ K}^{-1}$, and $\lambda = 0.630 \text{ W/m K}$. We never observed long transients like those reported by Chillà *et al.* (2004b) for $\Gamma = 0.5$ (see Brown *et al.* (2005)). On occasion we tilted the apparatus by 2° , and within our resolution of 0.1% found no effect on \mathcal{N} .

The results for \mathcal{N} and \mathcal{N}_{∞} are given in Tables 1 to 7 and are shown on logarithmic scales in Fig. 1a. With greater resolution they are shown in the compensated form $\mathcal{N}/R^{1/3}$ in

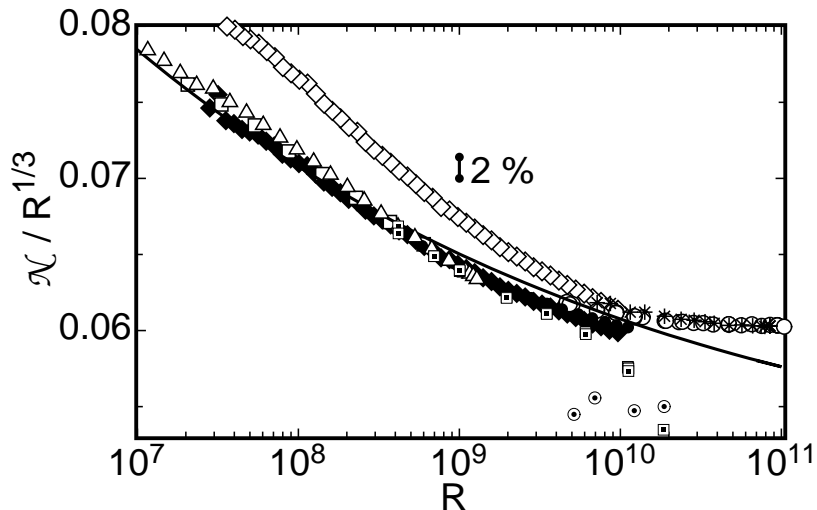


FIGURE 2. The reduced Nusselt number $\mathcal{N}_\infty/R^{1/3}$ or $\mathcal{N}/R^{1/3}$ on a linear scale as a function of the Rayleigh number R on a logarithmic scale for $\Gamma \simeq 1$. Stars (open circles): $\mathcal{N}_\infty/R^{1/3}$ for $\Gamma = 0.982$, $D = 49.7$ cm, run 1 (run2). Solid circles: $\mathcal{N}_\infty/R^{1/3}$ for $\Gamma = 1.003$, $D = 24.84$ cm. Open squares (triangles): $\mathcal{N}_\infty/R^{1/3}$ for $\Gamma = 0.967$, $D = 9.21$ cm, run 1 (run2). Open diamonds: $\mathcal{N}/R^{1/3}$ obtained with acetone ($\sigma = 3.96$, Xu, Bajaj & Ahlers(2000)) for $\Gamma = 1.004$ and $D = 8.74$ cm. Solid diamonds: $\mathcal{N}_\infty/R^{1/3}$ obtained from the acetone measurements after correction for the wall conductance (Ahlers(2000)). Open squares with solid dots: $\mathcal{N}/R^{1/3}$ obtained by Xia, Lam & Zhou(2002) using water with $\sigma = 4.29$. Open circles with solid dots: $\mathcal{N}/R^{1/3}$ obtained by Goldstein & Tokuda (1979) using water with $\sigma \simeq 6.2$. Solid line: the model of Grossmann & Lohse (2001) for $\Gamma = 1$ and $\sigma = 4.38$.

Fig. 1b. The results for $\Gamma = 0.982$ in Table 1 are not the same as those reported previously (run 1, Nikolaenko *et al.* (2005) Table 4; those results for \mathcal{N} and \mathcal{N}_∞ should be reduced by 0.5% because of an error in the area used in the original data analysis). They were taken in a second experiment (run 2) after the sample had been taken apart and re-assembled. Likewise, there are two separate runs for $\Gamma = 0.967$ in the small apparatus (Table 3) and for $\Gamma = 1.506$ in the large apparatus (Table 4). Within a given run the measurements were reproducible within one or two tenths of a percent (see, for instance, points 17 and 24 in Table 1). The two runs for $\Gamma = 1.506$ (Table 4) agree within their scatter of about 0.1%. On the other hand, the two runs with the large apparatus for $\Gamma = 0.982$ (Table 1 and Nikolaenko *et al.* (2005) Table 4), as well as the two runs from the small apparatus (Table 3), differ from each other by a few tenths of a percent, but by no more than expected possible systematic errors.

The results for $\Gamma \simeq 1$ from the small, medium, and large samples fall on nearly continuous smooth curves, but close inspection shows that there are small systematic offsets. The data lie close to the GL model (solid line). It is remarkable that the $\Gamma > 1$ data come so close to the $\Gamma \simeq 1$ results. For instance, the $\Gamma = 6$ values are only about 4% below the $\Gamma \simeq 1$ measurements. One assumes that the large- Γ sample had a much more complex large-scale-flow structure than the single circulating roll expected to exist for $\Gamma = 1$. Apparently this has only a very modest influence on the heat transport.

In Fig. 2 we compare the present results with previous measurements for $\Gamma \simeq 1$ and σ close to 4. Data for \mathcal{N} obtained using acetone ($\sigma = 3.96$) are shown as open diamonds [Xu, Bajaj & Ahlers(2000)]. The corresponding results obtained after a correction for the side-wall conductance [model 2, Ahlers(2000)] are given as solid diamonds. One sees

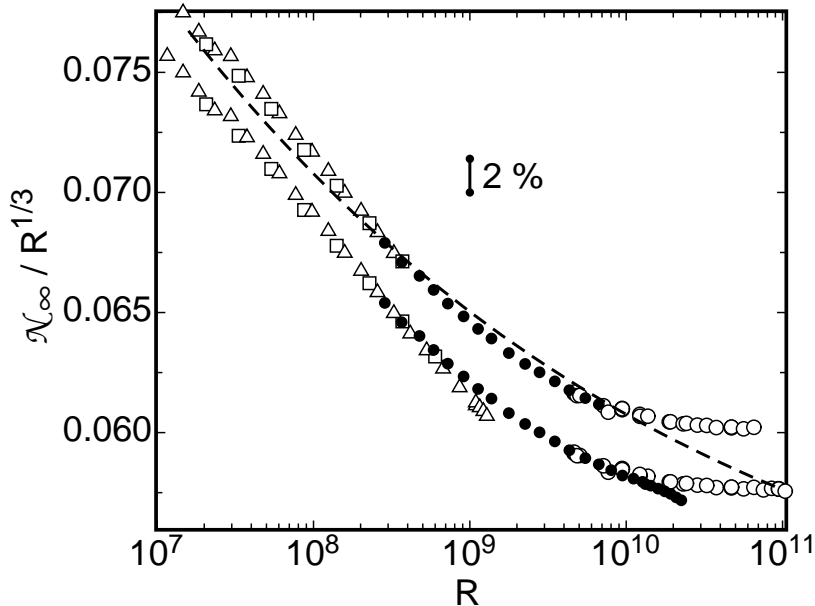


FIGURE 3. The reduced Nusselt number $\mathcal{N}_\infty/R^{1/3}$ on a linear scale as a function of the Rayleigh number R on a logarithmic scale. Open circles: $\Gamma = 0.982$, $D = 49.7$ cm, downshifted by 0.3%. Solid circles: $\Gamma = 1.003$, $D = 24.84$ cm, upshifted by 0.6%. Open triangle: $\Gamma = 0.967$, $D = 9.21$ cm, run 1, downshifted by 0.3%. Open squares: $\Gamma = 0.967$, $D = 9.21$ cm, run 2. Lower set: all data, moved down by 0.0025. Upper set: data that conform “strictly” to the Boussinesq approximation. Dashed line: the model of Grossmann & Lohse (2001) for $\Gamma = 1$ and $\sigma = 4.38$.

that in this case the wall correction is quite large, reaching about 8 % for $R = 10^8$ (no plate correction was required in this case, see Brown et al. (2005)). Nonetheless the corrected data for \mathcal{N}_∞ are in excellent overall agreement with the present results. The open squares with solid dots at their centers represent the results of Xia, Lam & Zhou(2002) using water with $\sigma = 4.29$. Up to $R \simeq 10^9$ they agree extremely well with the present measurements. For larger R they are slightly lower, presumably because of the influence of the finite plate conductivity. Also shown are data from Goldstein & Tokuda (1979). When corrections for the finite plate-conductivity (which had not been made) and the difference in σ are considered, they may be regarded as consistent with the present results.

3.2. Strictly Boussinesq data for $\Gamma \simeq 1$

The influence of departures from the Oberbeck-Boussinesq approximation (OBA) [Boussinesq (1903)] was considered by various authors. Most recently Niemela & Sreenivasan (2003) (NS) examined the issue in considerable detail in terms of various fluid properties. Unfortunately at present we have no theoretical criteria to decide whether a given variation over the applied temperature difference of a given property will affect \mathcal{N} significantly. Here we provide some insight into this problem from measurements with samples of different sizes but the same Γ .

Where they overlap, there is a small systematic offset between the $\Gamma \simeq 1$ data from the small sample, run 2 on the one hand and the medium-sample on the other. A similar offset exists between the data from the medium sample, and the large sample run 2. These offsets are well within possible experimental systematic errors. In order to obtain a single internally consistent data set spanning the entire range $10^7 \lesssim R \lesssim 10^{11}$, we shifted

$10^{-8}R$	\mathcal{N}_∞								
0.0921	16.55	0.1160	17.70	0.1464	18.95	0.1846	20.27	0.2334	21.69
0.2958	23.40	0.3753	25.04	0.4764	26.86	0.6052	28.78	0.7692	30.79
0.9785	33.04	1.2440	35.39	1.5830	37.86	2.0150	40.59	2.5650	43.42
3.2650	46.46								
0.1285	18.63	0.2058	21.23	0.3321	24.44	0.5370	28.13	0.8708	32.23
1.4070	37.00	2.2800	42.43	3.7010	48.69				
2.857	44.72	3.661	48.00	4.763	51.95	5.864	55.19	7.227	58.66
9.119	62.88	11.283	66.96	13.749	71.07	17.749	76.66	22.561	82.44
27.906	88.01	34.944	94.29	43.297	100.67	54.777	108.30	66.792	115.21
66.792	115.21								
46.36	102.79	46.42	102.90	48.42	104.11	50.55	105.63	71.55	117.77
76.73	120.02	94.20	128.84	94.20	128.75	94.26	128.78	94.33	128.87
122.18	139.94	122.39	139.84	137.57	145.40	188.56	160.89	192.00	161.87
231.37	172.01	242.66	174.83	284.99	184.23	327.32	192.89	376.98	201.89
470.65	217.34	471.05	217.50	471.35	217.56	563.10	230.58	655.73	242.84
655.73	242.84								

TABLE 8. Boussinesq results for $\Gamma = 1$. From top to bottom, the sections are for the small sample (run 1), small sample (run 2), medium sample, and large sample (run 2).

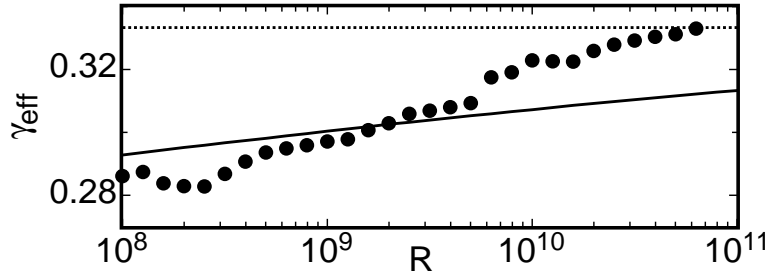


FIGURE 4. Effective exponent γ_{eff} of \mathcal{N}_∞ , determined from a powerlaw fit over a sliding window of half a decade in the strictly Boussinesq range, as a function of R . Dotted line: $\gamma_{eff} = 1/3$. Solid line: result of the GL model.

the data for \mathcal{N}_∞ from the small sample, run 2 downward by 0.3%. We also shifted the medium-sample data upward by 0.6%, and those from the large sample, run 2 downward by 0.3%. The result is shown by the lower sets of data (displaced downward by 0.0025 for clarity) in Fig. 3. The results from all three samples now merge smoothly into each other. We can then attribute the deviations of the small-sample data at their largest values of R from the medium-sample data to deviations from the OBA. A similar situation prevails with respect to the deviations of the medium-sample data from the large-sample results for $R \gtrsim 10^{10}$.

The upper sets of data in Fig. 3 (plotted without any vertical shift) consist only of those points, taken from the lower sets, that fall within approximately 0.2% of a smooth, continuous line through all the results. In Table 8 we give these points in numerical form. We regard these results as conforming “strictly” to the OBA. They are our best estimate of \mathcal{N}_∞ for $\sigma = 4.38$ and $10^7 \lesssim R \lesssim 10^{11}$, and constitute the primary result of our work.

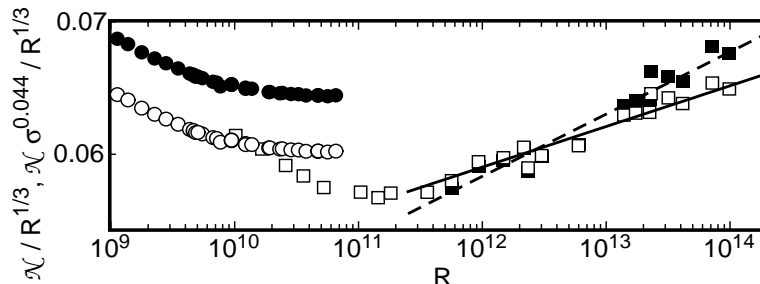


FIGURE 5. $\mathcal{N}/R^{1/3}$ (open symbols) and $\mathcal{N}\sigma^{0.044}/R^{1/3}$ (solid symbols) as a function of R on logarithmic scales for the present data (circles) and those of Niemela & Sreenivasan (2003) (squares).

3.3. The effective exponent γ_{eff} of $\mathcal{N}_\infty(R)$

A powerlaw $\mathcal{N}_\infty = N_0 R^{\gamma_{eff}}$ was fit to the data for $\mathcal{N}(R)$ in the strictly Boussinesq range (Table 8) within a sliding window covering half a decade of R . The results for γ_{eff} are shown in Fig. 4. Near $R = 10^8$ one sees that γ_{eff} has a value close to $2/7 \simeq 0.286$, the result of early theories (see, for instance, Siggia(1994)). With increasing R it increases linearly with $\log(R)$ within experimental error, reaching the large- R asymptotic value $\gamma_{eff} = 1/3$ of the GL model at the *finite* value $R_0 \simeq 7 \times 10^{10}$. Precision measurements conforming to the OBA for $\Gamma = 1, \sigma = 4.4$ and a wider range of R above R_0 are needed to determine whether γ_{eff} will remain at $1/3$.

As was seen in Fig. 3, the GL model is in reasonable agreement with the experimental results for $\mathcal{N}(R)$ up to $R \simeq 10^{10}$. However, for the model γ_{eff} increases somewhat more slowly with $\log(R)$ (solid line in Fig. 4) and reaches $1/3$ only in the limit as $R \rightarrow \infty$ whereas the experimental γ_{eff} becomes equal to $1/3$ at the finite $R_0 \simeq 7 \times 10^{10}$.

The result $\gamma_{eff} \simeq 1/3$ was obtained before by Goldstein & Tokuda (1979). However, they simultaneously fitted all their data, regardless of Γ , over the range $5 \times 10^8 \lesssim R \lesssim 3 \times 10^{11}$ to a power law, and found $\gamma_{eff} \simeq 1/3$ over the entire range. This is not in agreement with our results for $\Gamma = 1$ which yield an R -dependent γ_{eff} .

An exponent close to $1/3$ was found also by NS in experiments for $\Gamma = 1$ using helium gas where σ changed with R from about 1 to about 3.8. Those data (open squares) are displayed together with ours (open circles) in Fig. 5. Over the range $3 \times 10^{11} < R < 10^{14}$ they can be represented by a powerlaw with $\gamma_{eff} = 0.354$ (solid line) (when only data for $R > 10^{13}$ are fitted, one obtains $\gamma_{eff} = 0.345$). The σ -dependence of \mathcal{N} at constant R is not known very well. For $3.62 < \sigma < 5.42$, $\Gamma = 0.67$, and $R \simeq 10^{11}$ we have $\mathcal{N} \propto \sigma^{-0.044}$ [Nikolaenko *et al.* (2005)]. In order to see how much this could possibly influence the R -dependence, we also fitted the NS data for $\mathcal{N}\sigma^{0.044}$ (solid squares) and obtained $\gamma_{eff} = 0.365$ (dashed line). The results by NS, together with ours, suggest that γ_{eff} increases beyond $1/3$ as R grows beyond 10^{11} .

4. Acknowledgment

This work was supported by the US Department of Energy through Grant DE-FG02-03ER46080.

REFERENCES

- AHLERS, G. 2000 Effect of Sidewall Conductance on Heat-Transport Measurements for Turbulent Rayleigh-Benard Convection. *Phys. Rev. E* **63**, 015303-1-4(R).

- AHLERS, G., GROSSMANN, S. & LOHSE, D. 2002 Hochpräzision im Kochtopf: Neues zur turbulenten Konvektion. *Physik Journal* **1** (2), 31–37.
- AHLERS, G. & XU, X. 2001 Prandtl number dependence of heat transport in turbulent Rayleigh-Bénard convection. *Phys. Rev. Lett* **86**, 3320–3323.
- BOUSSINESQ, J. 1903 *Théorie Analytique de la Chaleur* (Gauthier-Villars, Paris).
- BROWN, E., NIKOLAENKO, A., FUNFSCHILLING, D., & AHLERS, G. 2005 Heat transport in turbulent Rayleigh-Bénard convection: Effect of finite top- and bottom-plate conductivity. Submitted to *Phys. Fluids*.
- CHAUMAT, S., CASTAING, B., & CHILLÀ, F. 2002 Rayleigh-Bénard cells: influence of the plates properties *Advances in Turbulence IX, Proceedings of the Ninth European Turbulence Conference*, edited by I.P. Castro and P.E. Hancock (CIMNE, Barcelona) .
- CHILLÀ, F., RASTELLO, M., CHAUMAT, S., & CASTAING, B. 2004a Ultimate regime in Rayleigh-Bénard convection: The role of the plates. *Phys. Fluids* **16**, 2452–2456.
- CHILLÀ, F., RASTELLO, M., CHAUMAT, S., & CASTAING, B. 2004b Long relaxation times and tilt sensitivity in Rayleigh-Bénard turbulence. *Euro. Phys. J. B* **40**, 223–227.
- GOLDSTEIN, R.J. & TOKUDA, S. 1979 Heat transfer by thermal convection at high Rayleigh numbers. *Int. J. Heat Mass Transfer* **23**, 738–740.
- GROSSMANN, S. & LOHSE, D. 2000 Scaling in thermal convection: A unifying view. *J. Fluid Mech.* **407**, 27–56.
- GROSSMANN, S. & LOHSE, D. 2001 Thermal convection for large Prandtl number. *Phys. Rev. Lett.* **86**, 3317–3319.
- GROSSMANN, S. & LOHSE, D. 2002 Prandtl and Rayleigh number dependence of the Reynolds number in turbulent thermal convection. *Phys. Rev. E.* **66**, 016305.
- GROSSMANN, S. & LOHSE, D. 2003 On geometry effects in Rayleigh-Bénard convection. *J. Fluid Mech.* **486**, 105–114.
- GROSSMANN, S. & LOHSE, D. 2004 Fluctuations in turbulent Rayleigh-Bénard convection: the role of plumes. *Phys. Fluids* **16**, 4462–4472.
- KADANOFF, L. P. 2001 Turbulent heat flow: Structures and scaling. *Phys. Today* **54** (8), 34–39.
- KRAICHNAN, R. 1962 Turbulent thermal convection at arbitrary Prandtl number. *Phys. Fluids* **5**, 1374–1389.
- NIEMELA, J. & SREENIVASAN, K. R. 2003 Confined turbulent convection. *J. Fluid Mech.* **481**, 355–384.
- NIKOLAENKO, A. & AHLERS, G. 2003 Nusselt number measurements for turbulent Rayleigh-Bénard convection. *Phys. Rev. Lett* **91**, 084501-1–4.
- NIKOLAENKO, A. , BROWN, E., FUNFSCHILLING, D., & AHLERS, G. 2005 Heat transport by turbulent Rayleigh-Bénard Convection in cylindrical cells with aspect ratio one and less. *J. Fluid Mech.* **523**, 251–260.
- ROCHE, P., CASTAING, B., CHABAUD, B., HEBRAL, B., & SOMMERIA, J. 2001 Side wall effects in Rayleigh-Bénard experiments. *Europhys. J. B* **24**, 405–408.
- SIGGIA, E. D. 1994 High Rayleigh number convection. *Annu. Rev. Fluid Mech.* **26**, 137–168.
- VERZICCO, R. 2002 Side wall finite-conductivity effects in confined turbulent thermal convection. *J. Fluid Mech.* **473**, 201–210.
- VERZICCO, R. 2004 Effects of non-perfect thermal sources in turbulent thermal convection. *Phys. Fluids* **16**, 1965–1979.
- VERZICCO, R. & CAMUSSI, R. 2003 Numerical experiments on strongly turbulent thermal convection in a slender cylindrical cell. *J. Fluid Mech.* **477**, 19–49.
- XIA, K.-Q., LAM, S. & ZHOU, S.-Q. 2002 Heat-flux measurements in high-Prandtl-number Rayleigh-Bénard convection. *Phys. Rev. Lett.* **88**, 064501-1–4.
- XU, X., BAJAJ, K. M. S. & AHLERS, G. 2000 Heat transport in turbulent Rayleigh-Bénard convection. *Phys. Rev. Lett.* **84**, 4357–4360.